OPTIMAL AND EFFICIENT SEGMENTATION FOR 3D VASCULAR FOREST STRUCTURE WITH GRAPH CUTS

Ning Zhu and Albert C.S. Chung

Lo Kwee-Seong Medical Image Analysis Laboratory,
Department of Computer Science and Engineering,
The Hong Kong University of Science and Technology, Hong Kong.

ABSTRACT

In this paper, we propose an optimal segmentation method for vascular forest structure based on graph cuts framework, which has widely been used in recent years because of its global optimal object segmentation property. However, shrinking bias, a classical issue of the graph cuts methods, sets up a barrier for the use of these methods on elongated structures such as blood vessels, especially the complex vascular tree and forest structures. To deal with this problem, a new graph construction method and a new energy function are proposed in this paper. The global optimal segmentation of vascular forest structure can be obtained more efficiently, while the shrinking bias can be overcome by the proposed method. The method is compared with a classical graph cuts method [1] and two methods [2, 3] for vascular tree structure segmentation, and is demonstrated to be more accurate on both the synthetic and clinical images, especially on noisy images. Different from many other tree structure segmentation methods, the proposed method does not have to consider the bifurcations explicitly.

Index Terms— Graph Cuts, Optimal Segmentation, 3D Vascular Forest

1. INTRODUCTION

In recent years, minimum graph cuts (min-cut) framework has become a widely used technique for object segmentation [1, 4, 5, 6, 7, 8]. As described in [1], different from other popular segmentation methods, such as snakes, geodesic active contours and methods based on level-set, min-cut/max-flow method can be used to obtain global optimal segmentation from computationally efficient energy minimization. However, the min-cut methods aim at minimizing the sum of the cuts' weights for a graph, and it is prone to have smaller (thinner and shorter) resultant segmentation surfaces. This problem, namely shrinking bias [9, 10], is especially obvious for segmenting elongated structures [9, 11]. Segmentation methods in [6, 7, 8] used min-cut method to obtain optimal surface for single branch vessel. However, for the whole vessel tree, a simple combination of different branch surfaces may not work reliably, especially in the areas of bifurcation. To the best of our knowledge, there are only a few methods [2, 3] for vessel tree segmentation based on the min-cut framework due to the shrinking bias for elongated structures, especially the complex vascular tree structure. In these two methods [2, 3], tubular structure segments in the whole volume are first detected and then the segmentations are obtained with the min-cut method. The exhaustive forest detection may lead to the unwanted tiny vessel branches and noisy tissue being included in the reconstructed vessel tree.

In this paper, we show that accurate segmentation of vascular forest structure can be obtained with the proposed method. There are four favorable properties of the proposed method. (i) With the new energy term incorporating the tubular prior and the new graph construction method, the proposed method can avoid the shrinking bias which is a classical issue of the graph cuts methods. (ii) The proposed method is highly computationally efficient. The new graph construction method eliminates the unrelated voxels, and also deletes the edges connecting seed points. These make the proposed method a highly computationally efficient method without affecting the segmentation performance. (iii) Different from many other tree structure segmentation methods, bifurcations do not require particular consideration with the proposed method. (iv) The segmentation result is global optimal thanks to the min-cut/max-flow framework exploited.

2. OPTIMAL SEGMENTATION FOR VASCULAR FOREST STRUCTURE

For min-cut methods, graph construction and energy function are the two major factors affecting the segmentation performance. In this method, a new graph construction and a new energy function are proposed to obtain an optimal segmentation efficiently while eliminating the shrinking bias.

2.1. Multiple Sources and Sinks Graph Construction

The proposed graph construction method is described in Algorithm 1. To avoid the shrinking bias and make the segmentation more efficient, the centerlines of the forest struc-

Algorithm 1: Graph Construction for Forest Segmentation

Require: IV – image voxels, $Seeds$ – seed points for finding centerline, m – multiple factor, δ – small threshold.

1: **for** each voxel IV_i in IV, **do** $Label(IV_i)$ =U.
2: Find the centerline points (C) and associate radii (R) of the forest structure with $Seeds$ using method in [12].
3: **for** each voxel C_i in set C **do** $Label(C_i)$ = S.
4: **for** each voxel IV_j with its distance from C_i, $dis(IV_j, C_i) \leq m * R_i + \delta$ **do**
5: **if** $|\text{dis}(IV_j, C_i) - m * R_i| \leq \delta$ & $Label(IV_j)$ =U
6: **then** $Label(IV_j)$ =T
7: **else if** $\text{dis}(IV_j, C_i) < m * R_i - \delta$ & $Label(IV_j)$! =S
8: **then** $Label(IV_j)$ =B
9: **end for**
10: **end for**
11: $V = \{IV_i | Label(IV_i) = \{S, T, B\}\} \bigcup SS \bigcup ST$, $E = \{e(V_i, V_j) | e(V_i, V_j) \in N\} \bigcup \{e(SS, S_i)\} \bigcup \{e(T_j, ST)\}$, where N is the set of edges consisting of neighboring nodes, S_i and T_j are nodes labeled as S and T.
12: **return** $G = \{V, E\}$

ture are first extracted. Without sufficient information about the elongated structure, the graph cut method has preference for finding a shorter segment since it aims at minimizing the sum of weights on the cuts of the graph. The shrinking bias can be solved if the centerline points are given as seeds. After obtaining the centerline and the reference radii, all voxels in the image are labeled as either sources (labeled S, centerline points), sinks (labeled T, outer boundary points), graph nodes (labeled B, points in between), or unrelated points (labeled U) according to Algorithm 1 with 26-neighborhood connectivity. The geometric relation between different kinds of points are sketched in Fig.1(a) and the constructed directed graph is shown in Fig.1(b). A super source (SS) connected to all sources and a super sink (ST) connected to all sinks are also added for implementation purpose. The proposed graph construction method eliminates the unrelated voxels while including all possible voxels in the vascular forest and the voxels nearby. As a result, the computation efficiency is improved significantly while the segmentation performance is not affected. In some cases, the accuracy is even higher since the unrelated noisy parts are excluded. The output of the algorithm is just a graph structure, and the directed graph edge weights are then set according to Table 1. With the graph structure and edge weights, min-cut/max-flow optimization [13, 14] is applied to obtain the optimal segmentation.

2.2. Cost Function

As we have mentioned in Section 1, the segmentation performance also depends on the cost function of the graph. Given a graph $G(V, E)$, the following energy framework is used in energy-based min-cut methods,

$$E(L) = \lambda_1 \cdot E_A(L) + \lambda_2 \cdot E_B(L), \tag{1}$$

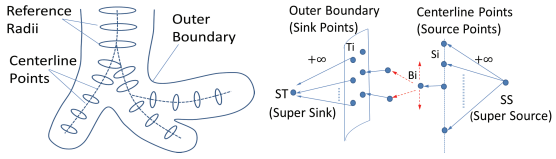

(a) Geometric relation (b) Graph construction

Fig. 1. Multiple Sources and Sinks

in which, $L = \{L_i, 1 \leq i \leq |V|\}$ represents the label set of all nodes in G. L_i can be either "vessel" or "background", different from the initialization labels(S,T,U,B) in Algorithm 1 which aims at selecting candidate nodes and providing initialization for min-cut method, L here is the result label set obtained with min-cut method by optimizing energy term in Equation 1. $E_A(L)$ and $E_B(L)$ represents the regional term and boundary term respectively. $E_A(L)$ represents the sum of penalty for assigning the voxels to the label set L. In most cases, the penalty is defined only according to the intensity histogram, such as [1, 3]. In the proposed method, we define a new formulation of $E_A(L)$, which incorporates both intensity histogram and vessel shape information.

$$\begin{aligned} E_A(L) &= \sum_{1 \leq i \leq |V|} E_A(L_i) \\ &= \sum_{1 \leq i \leq |V|} \frac{Pv(\bar{L_i}, v_i) \cdot H(\bar{L_i}, I_i)}{Pv(L_i, v_i) \cdot H(L_i, I_i) + Pv(\bar{L_i}, v_i) \cdot H(\bar{L_i}, I_i)}. \end{aligned} \tag{2}$$

H here gives two intensity histograms for "vessel" and "background". The histograms are normalized by the sum of the density, so they represent the probability density given the intensity. $\bar{L_i}$ means the opposite label of L_i. Here we change the dual-sigmoidal filter from [15] and make it as $Pv(L_i, v_i)$. Different from [15], in which the dual-sigmoidal filter is used as an intensity refractive index for wave propagation, we use the new filter $Pv(L_i, v_i)$ as the prior probability of v_i being "vessel" or "background".

$$Pv(L_i, v_i) = \begin{cases} \frac{1}{1+\exp(\tau)} & \text{if } L_i = \text{“}background\text{”}; \\ \frac{1}{1+\exp(-\tau)} & \text{if } L_i = \text{“}vessel\text{”}, \end{cases} \tag{3}$$

$$\tau = a \cdot (\text{dis}(v_i, c_j) - R_j);$$

Here $\text{dis}(v_i, c_j)$ is the distance between v_i and associated centerline point c_j, R_j is the reference radius of c_j, and a can be viewed as the slope of the filter. $Pv(L_i, v_i)$ is a good vessel indicator given the reference radius. The sum of $Pv(\text{“}vessel\text{”}, v_i)$ and $Pv(\text{“}background\text{”}, v_i)$ is 1 for each v_i, and when the distance between v_i and c_j is R_j, the prior probability of node v_i being a vessel point is 0.5. $E_B(L)$ in Equation 1 is defined similar to the boundary term in [1],

$$E_B(L) = \sum_{e\{B_i, B_j\} \in N} E_{Bi,Bj} \cdot \delta_{L_{Bi} \neq L_{Bj}};$$

$$E_{Bi,Bj} = \begin{cases} \exp\left(-\frac{\nabla^2}{2\omega^2}\right) \cdot \mathrm{dis}(B_i, B_j)^{-1} & \text{if } I_i > I_j; \\ 1 & \text{if } I_i <= I_j. \end{cases} \quad (4)$$

∇ is the intensity difference. After defining the energy terms in Equation 1 as optimization objective, we now give the details of edge weight assignment in Table 1. With these weights assigned to the directed edges in the constructed graph, the energy term in Equation 1 can be optimized with the min-cut method.

Different with some other applications in which region of interest is easy to extract, 3D coordinates of vascular forest structure spread over large area and the structure is complex. With this new graph construction method, unrelated points (labeled U) in the image are eliminated; otherwise, it may be demanding on RAM and the computation time will be really long. For example, with the proposed method, only around 500,000 nodes are considered for a image with its size 512*512*288 when the multiply factor m is set to 2. The time complexity for running the Ford-Fulkerson Algorithm is $O(|E| \cdot |f*|)$. Obviously, $|f*|$, the value of maximum flow, becomes smaller if the number of nodes is smaller. $|E|$ is the number of edges, and it is in proportion to $|V|$ in our graph. As a result, the time complexity of the proposed method is at most 1/150 of the methods considering all voxels in the image. In the mean time, the proposed multiple source and sink graph construction method does not have edges within seed sets (S and T), which also reduces the number of edges remarkably.

The new region energy term exploited in this method incorporates the new sigmoidal filter as the prior probability of nodes being either "vessel" or "background". This improves the reliability of the segmentation and also helps to avoid the problem of shrinking. The shrinking along the elongated direction is avoided by using the obtained centerlines, which outline the skeleton of the forest structure.

Table 1. Edge Weights

	Directed Edges	Cost
Boundary Energy	e$\{B_j, B_p\}$	$\lambda_2 E_{B_i,B_j}$
Region Energy	e$\{SS, B_j\}$	$\lambda_1 E_A(L_{B_j} = \text{“}background\text{”})$
	e$\{B_j, ST\}$	$\lambda_1 E_A(L_{B_j} = \text{“}vessel\text{”})$
Other Setting	e$\{S_i, B_j\}$,e$\{B_j, T_k\}$, e$\{SS, S_i\}$,e$\{T_k, ST\}$	∞

3. EXPERIMENT AND VALIDATION

For method evaluation, we compared the proposed method with three related methods in [1, 2, 3] on both synthetic images and clinical CTA images. Since the method in [1] is not designed for tree nor forest structure segmentation, the comparison with this method is only carried out on synthetic image 1. The other two methods, to the best of our knowledge, are the only existing methods for vascular forest structure segmentation based on min-cut framework.

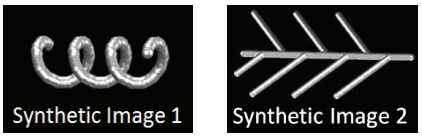

Fig. 2. Synthetic Images

The method in [2] construct a graph for ROI, which is a essential step for skeleton based graph cuts methods. There are differences between the method in [2] and our method in both cost function and graph construction. As for graph construction, the proposed method uses centerline points as source points and a outer boundary with radius $m * R$ as sink points, while [2] uses a constant d_m as the distance between sources and estimated surface, and also for estimated surface and sinks. Another difference is that in the proposed method, we do not have graph edges within the source points set and also the sink points set. This is reasonable and the graph obtained may have much less edges, which makes the optimization more efficient. In all experiments, for the sake of fairness, the same set of seed points (S and T), and the graph constructed with the proposed method were given to all methods as initialization. These seed points should be adequate for all methods [1, 2, 3] to obtain accurate results. For the proposed method, we set $\lambda_1 = \lambda_2 = 1$, the slope of the new sigmoidal filter (Equation 3) $a = 2$, and multiple factor $m = 2$ in all experiments on both the synthetic images and real images. While ω in Equation 4 was set to 200 in the synthetic experiments and 20 for the real images because this parameter is closely related to image intensity range. For the other three methods, all parameters were set according to the original parameters given in the papers, except the ωs, which should be adjusted according to the image data. And the setting of ωs are same as the setting of the proposed method.

Table 2. Accuracy on Synthetic Image 1

σ (noise level)	200	400	600	800	1000
Our method	100%	99.67%	97.98%	93.63%	91.61%
Boykov et.al., 2006 [1]	100%	99.84%	93.25%	89.79%	85.78%

The synthetic vascular images (Fig.2) were generated by setting the vessel intensity to 1200 and background intensity to 800. Gaussian noise was added to this synthetic image to generate a series of noisy synthetic images. The experimental results for method comparison on synthetic images are listed in Table 2 and Table 3. The accuracy is calculated as the percentage of the nodes that are labeled correctly. As listed in the tables, as the noise level increases, the accuracy of methods in [1, 2, 3] decreases quickly while the proposed method still gives accurate segmentations. In [1], both the boundary energy and regional energy are only based on intensities. For the method in [2], only boundary energy which represents the

Table 3. Accuracy on Synthetic Image 2(σ is noise level)

	WithoutNoise	$\sigma = 100$	$\sigma = 200$	$\sigma = 250$	$\sigma = 300$	$\sigma = 350$	$\sigma = 400$
Our method	100%	100%	99.8246%	98.8296%	97.0342%	95.3358%	94.1446%
Bauer et.al., 2010 [2]	100%	95.8611%	95.858%	95.8035%	93.6116%	91.2567%	84.2667%
Esneault et.al., 2010 [3]	100%	100%	99.822%	99.0616%	96.1051%	88.4362%	79.3804%

changes between neighboring nodes is used. Without the help of regional energy, the method may not be robust when the noise level increases. Vessel energy term used in [3] needs to compete with the boundary energy, region energy when the noise level increases. Different from these methods, we incorporate the new sigmoidal prior probability of nodes being "vessel" or "background" in the region energy, and this increases the robustness of the proposed method.

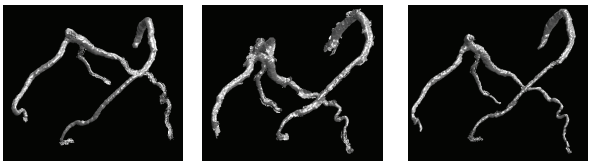

(a) Result for [2] (b) Result for [3] (c) Our method

Fig. 3. Segmentation Results for Real CTA Image

Experiments have also been carried out on real CTA images for coronary artery segmentation. For visualization and evaluation, we transformed the implicit segmentation results into explicit boundaries by finding points with both "vessel" and "background" neighbors. Fig. 3 presents a comparison of rendering results of coronary artery forest boundaries obtained with our method and the methods in [2, 3]. The rendering surfaces of our method are smoother than those of the other two method. And Fig. 4 shows some resultant slides obtained with the three methods. The surfaces for [2] seems smoother than that of [3], however, without the help of regional energy, the method in [2] may suffer from shrinking problem, which makes some distal part thinner than the real segmentation and the rendering surface is hackly as shown in Fig. 3.

The experiments on the synthetic images and the clinical data demonstrate that the proposed method performs better than the other methods thanks to the newly proposed energy terms. It should be noted that with the proposed method, forest structure segmentation can be optimized altogether. As such, different from vascular tree and forest segmentation methods, bifurcation areas do not require particular consideration.

The optimization procedure for a coronary artery forest with 4 major branches in a 512*512*288 CTA image can be done within 2 seconds on a laptop with a 2.6 GHz processor and 8GB RAM. While as reported in [1], objects in the images with size about 1/10 to 1/20 of our images can be segmented in 10-30 seconds. This result gives a similar demonstration with the theoretical computation complexity discussed in Section 2.2 that the time complexity of the proposed method is about 1/150 of the methods considering all voxels in the image.

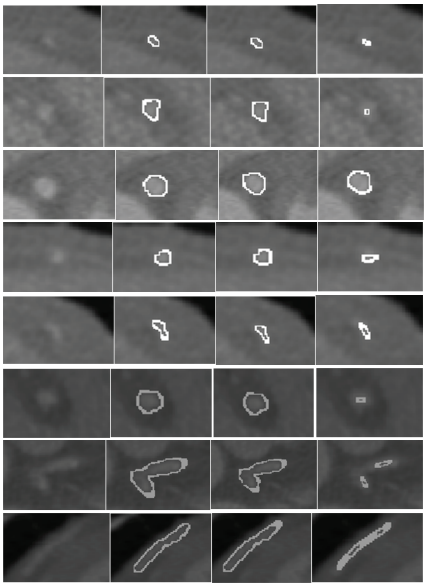

Fig. 4. Comparison of Segmentation Result Slides. (from left to right: the original image, the results of our method, [3] and [2].)

4. CONCLUSION

In this paper, we have proposed an optimal segmentation method for vascular forest structure based on graph cuts framework. To solve the shrinking bias problem, a new graph construction method and a new energy function are proposed in this paper. The global optimal segmentation of tubular forest structure can be obtained more efficiently, while the shrinking bias can be overcome by the proposed method. The method has been compared with the classical graph cuts method [1] and two methods [2, 3] for vascular forest structure segmentation on both synthetic and clinical images, and has been shown to be more accurate than these methods, especially on noisy images. The computation efficiency is about 1/150 of the methods considering all voxels in the image.

We would like to acknowledge the financial support of the Hong Kong Research Grants Council under grant 612011.

5. REFERENCES

[1] Y. Boykov and G. Funka-Lea, "Graph cuts and efficient nd image segmentation," *International Journal of Computer Vision*, vol. 70, no. 2, pp. 109–131, 2006.

[2] C. Bauer, T. Pock, and et al., "Segmentation of interwoven 3d tubular tree structures utilizing shape priors and graph cuts," *Medical Image Analysis*, vol. 14, no. 2, pp. 172–184, 2010.

[3] S. Esneault, C. Lafon, and et al., "Liver vessels segmentation using a hybrid geometrical moments/graph cuts method," *IEEE Transactions on Biomedical Engineering*, vol. 57, no. 2, pp. 276–283, 2010.

[4] Y.Y. Boykov and M.P. Jolly, "Interactive graph cuts for optimal boundary & region segmentation of objects in nd images," in *Eighth IEEE International Conference on Computer Vision–ICCV*, 2001, vol. 1, pp. 105–112.

[5] L. Grady and M.P. Jolly, "Weights and topology: A study of the effects of graph construction on 3d image segmentation," in *Medical Image Computing and Computer-Assisted Intervention–MICCAI*, 2008, pp. 153–161.

[6] K. Li, X. Wu, and et al., "Optimal surface segmentation in volumetric images-a graph-theoretic approach," *IEEE Transactions on Pattern Analysis and Machine Intelligence*, vol. 28, no. 1, pp. 119–134, 2006.

[7] M. Schaap, L. Neefjes, and et al., "Coronary lumen segmentation using graph cuts and robust kernel regression," in *Information Processing in Medical Imaging*, 2009, pp. 528–539.

[8] F. Zhao, H. Zhang, and et al., "Congenital aortic disease: 4d magnetic resonance segmentation and quantitative analysis," *Medical Image Analysis*, vol. 13, no. 3, pp. 483–493, 2009.

[9] S. Vicente, V. Kolmogorov, and C. Rother, "Graph cut based image segmentation with connectivity priors," in *IEEE Conference on Computer Vision and Pattern Recognition–CVPR*, 2008, pp. 1–8.

[10] K. Kolev and D. Cremers, "Continuous ratio optimization via convex relaxation with applications to multiview 3d reconstruction," in *IEEE Conference on Computer Vision and Pattern Recognition–CVPR*, 2009, pp. 1858–1864.

[11] D. Singaraju, L. Grady, and et al., "P-brush: Continuous valued mrfs with normed pairwise distributions for image segmentation," in *IEEE Conference on Computer Vision and Pattern Recognition–CVPR*, 2009, pp. 1303–1310.

[12] N. Zhu and A. Chung, "Minimum average-cost path for real time 3d coronary artery segmentation of ct images," in *Medical Image Computing and Computer-Assisted Intervention–MICCAI*, 2011.

[13] L.R. Ford and D.R. Fulkerson, "Maximal flow through a network," *Can.J.Math.*, pp. 399–404, 1956.

[14] Y. Boykov and V. Kolmogorov, "An experimental comparison of min-cut/max-flow algorithms for energy minimization in vision," *IEEE Transactions on Pattern Analysis and Machine Intelligence*, vol. 26, no. 9, pp. 1124–1137, 2004.

[15] F.K.H. Quek and C. Kirbas, "Vessel extraction in medical images by wave-propagation and traceback," *IEEE Transactions on Medical Imaging*, vol. 20, no. 2, pp. 117–131, 2001.